Electronic Supplementary Material (ESI) for Journal of Materials Chemistry A.

Electronic Supplementary Information

Novel Graphitic Carbon Nitride *g*-C_9N_{10} as Promising Platform to Design Efficient Photocatalyst for Dinitrogen Reduction to Ammonia: The First Principle Investigation

Lixue Xia,[a] Huan Wang,*[b] Yan Zhao*[ac]

[a]*State Key Laboratory of Silicate Materials for Architectures, International School of Materials Science and Engineering, Wuhan University of Technology, No. 122 Luoshi Road, Wuhan 430070, P. R. China.*

[b]*State Key Laboratory of Advanced Technology for Materials Synthesis and Processing, Center of Smart Materials and Devices, School of Materials Science and Engineering, Wuhan University of Technology, No. 122 Luoshi Road, Wuhan 430070, P. R. China*

[c]*The Institute of Technological Sciences, Wuhan University, No. 199 Bayi Road, Wuhan 430072, P. R. China.*

**E-mail: huan.wang@whut.edu.cn*

yan2000@whut.edu.cn

Table of Contents

Feasible Synthesis Scheme for *g*-C_9N_{10}

Two experimentally synthesized carbon nitrides, *g*-CN and *g*-C_6N_7, may provide us more insight into the synthesis of *g*-C_9N_{10}. As a 2D carbon nitride which has been applied in various field, *g*-CN (see Figure S1a) was firstly experimentally synthesized through a simple solvothermal method by Li et. al. in 2006.[1] The *g*-C_6N_7 (see Figure S1b), a novel C–C bridged heptazine, was synthesized by Zhao et. al. using urea and oxamide as precursor.[2] There are several common features between *g*-CN and *g*-C_6N_7, such as the same P-6m2 space group, the C-C bridge between two basic unit, which demonstrates that C_3N_3 and C_6N_7 can serve as stable structure unit to form 2D carbon nitride. Furthermore, the C_3N_3 and C_6N_7 exhibit the high structural similarity that each C_6N_7 consists of three C_3N_3 ring, which provides high possibility for them to bond with each other and form g-C_9N_{10} (see Figure S1c). For the synthesis of *g*-CN reported by Li et al.[1] (shown in Figure 1d), a simple solvothermal method through the reaction of $C_3N_3Cl_3$ and Sodium (Na) was conducted at different temperature with different time to obtain *g*-CN with various morphology. Inspired by this method, we rationally propose a feasible synthetic scheme for *g*-C_9N_{10}. Similarly, the commercially available heptazine chloride ($C_6N_7Cl_3$) and cyanuric chloride ($C_3N_3Cl_3$) serve as precursors to react with Na through a simple solvothermal method as shown in Figure S1e. It should be noted that $C_6N_7Cl_3$ and $C_3N_3Cl_3$ have been wildly used as precursors for synthesis.[1, 3-5] More importantly, the synthetic condition, such as temperature, pressure, and reaction time, may need to modify to ensure that the C_6N_7 and C_3N_3 rings would connect with each other rather than itself. The products of *g*-C_9N_{10} and NaCl would obtain. Thus, the existence and synthesis of *g*-C_9N_{10} holds high possibility.

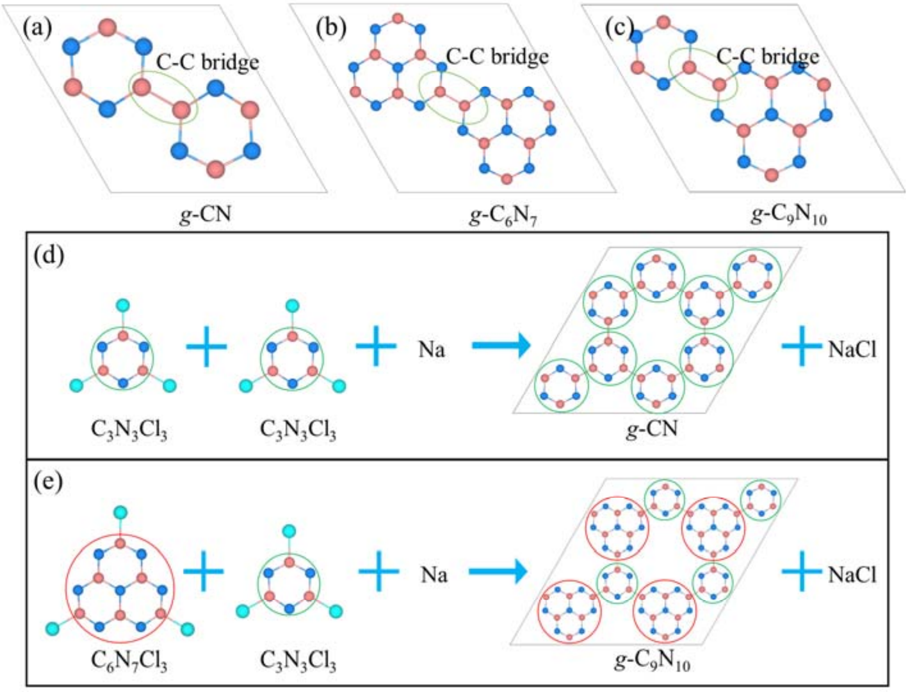

Figure S1. The configuration of three carbon nitride, (a) *g*-CN, (b) *g*-C_6N_7, (c) *g*-C_9N_{10}. The red and blue balls represent the carbon and nitrogen atoms, respectively. (d) The schematic synthesis process of *g*-CN reported by Li et. al.[1] (e) The feasible synthetic method of g-C_9N_{10}. The red, blue, and cyan balls represent the carbon, nitrogen, and chlorine atoms, respectively.

Table S1. Zero-point energy (ZPE, eV), entropy (*TS*, eV) of different adsorption species and corresponding energy correction to Gibbs free energy (*G*), where * denoted the adsorption site.

Species	**ZPE**	***TS***	***G***
H_2	0.30	0.40	−0.11
N_2	0.16	0.59	−0.43
NH_3	0.94	0.60	0.34
$*N_2$	0.23	0.13	0.10
*NNH	0.52	0.14	0.38
$*NNH_2$	0.86	0.12	0.74
$*NNH_3$	1.21	0.12	1.09
*NHNH	0.85	0.13	0.72
$*NHNH_2$	1.20	0.14	1.06
$*NH_2NH_2$	1.49	0.15	1.34
*NH	0.39	0.06	0.32
$*NH_2$	0.75	0.07	0.68
$*NH_3$	1.02	0.08	0.93
*N-*N	0.21	0.11	0.10
*N-*NH	0.51	0.11	0.40
*NH-*NH	0.83	0.11	0.72
$*NH*NH_2$	1.08	0.15	0.93
$*NH_2*NH_2$	1.43	0.20	1.24
*H	0.19	0.17	0.01

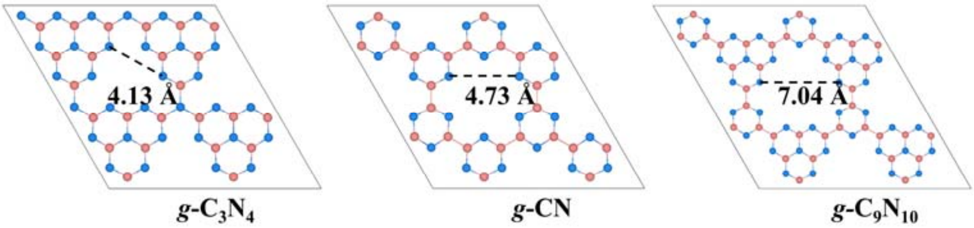

Figure S2. The correspond structure of *g*-C_3N_4, *g*-CN and *g*-C_9N_{10}. The distance of nitrogen in two binding site is shown in structure. The pink and blue balls denote carbon and nitrogen atoms, respectively.

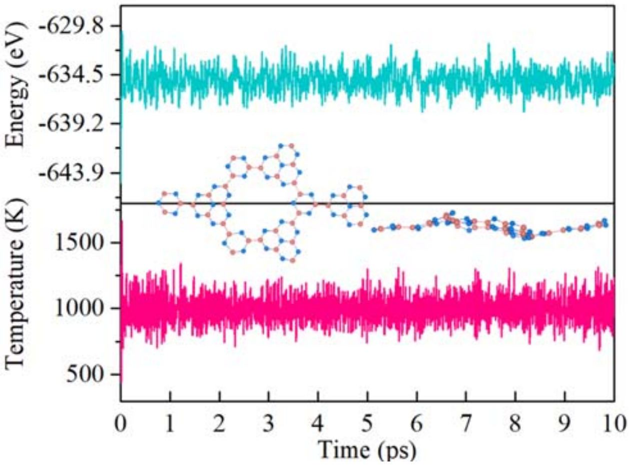

Figure S3. Energy and temperature variation against AIMD time of *g*-C_9N_{10} for 10 ps at 1000 K.

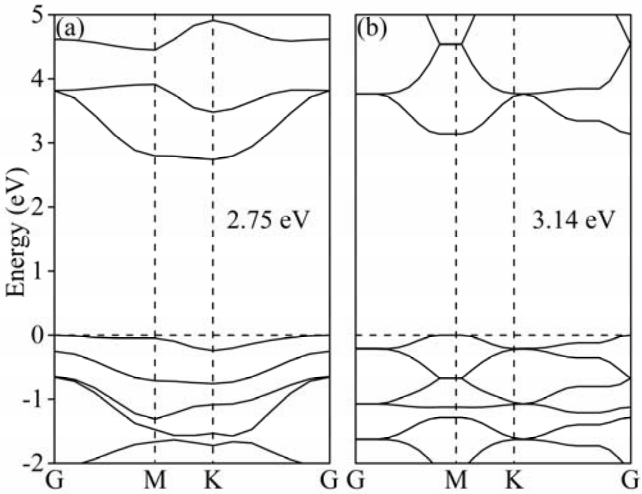

Figure S4. The band structure of (a) *g*-C_3N_4 and (b) *g*-CN by HSE06 functional.

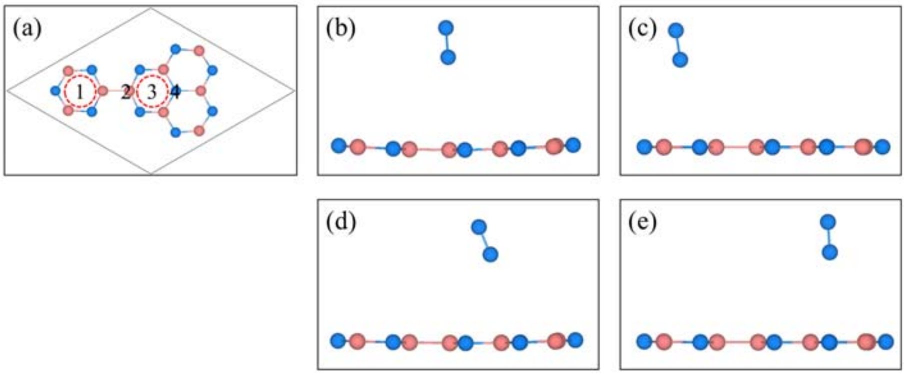

Figure S5. (a) Four initial N_2 adsorption site on pristine *g*-C_9N_{10}. (b), (c), (d) and (e) are corresponding configuration after geometry optimization. The pink and blue balls denote carbon and nitrogen atoms, respectively.

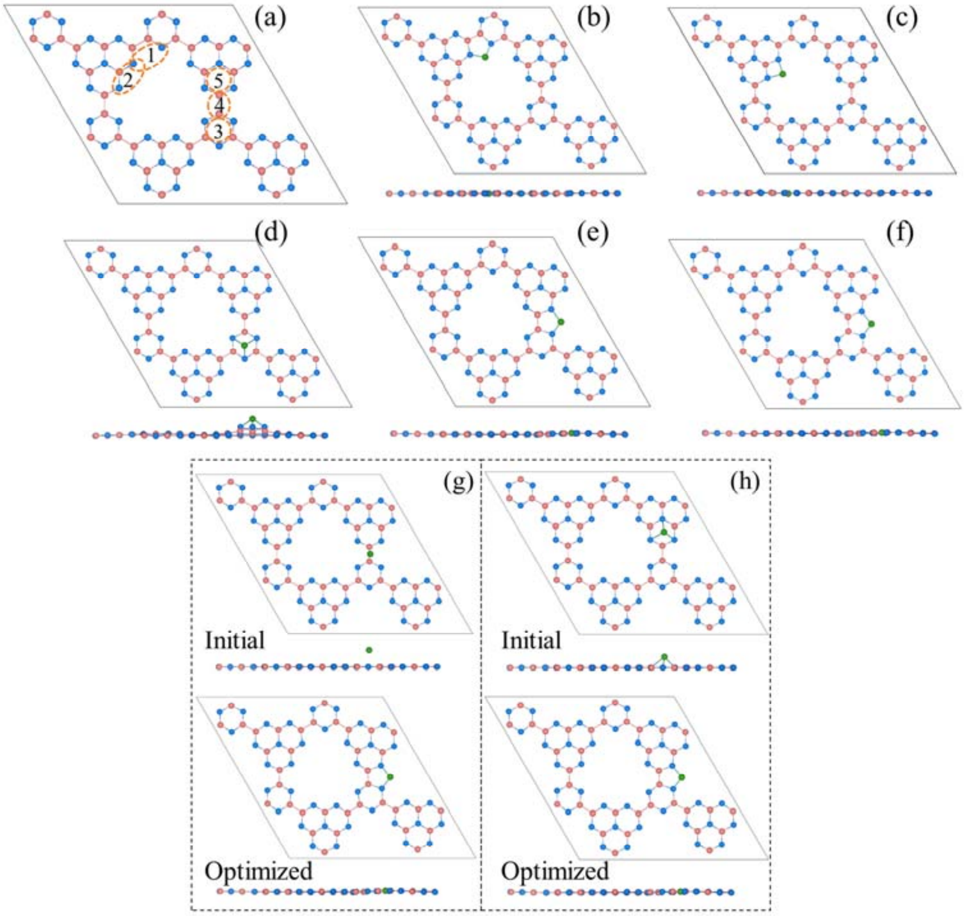

Figure S6. (a) Five possible B anchoring site. (b)-(f) are the corresponding optimized structures. The initial and optimized configuration of B adsorbed on (g) site 4 and (h) site 5. The pink, blue, and green balls denote carbon, nitrogen, and boron atoms, respectively.

Table S2. The binding energy of B atom on five possible sites of *g*-C_9N_{10}. The symbol / denotes that the B atom move to the most stable site.

Site	1	2	3	4	5
E_b (eV)	−5.89	−3.46	−0.31	/	/

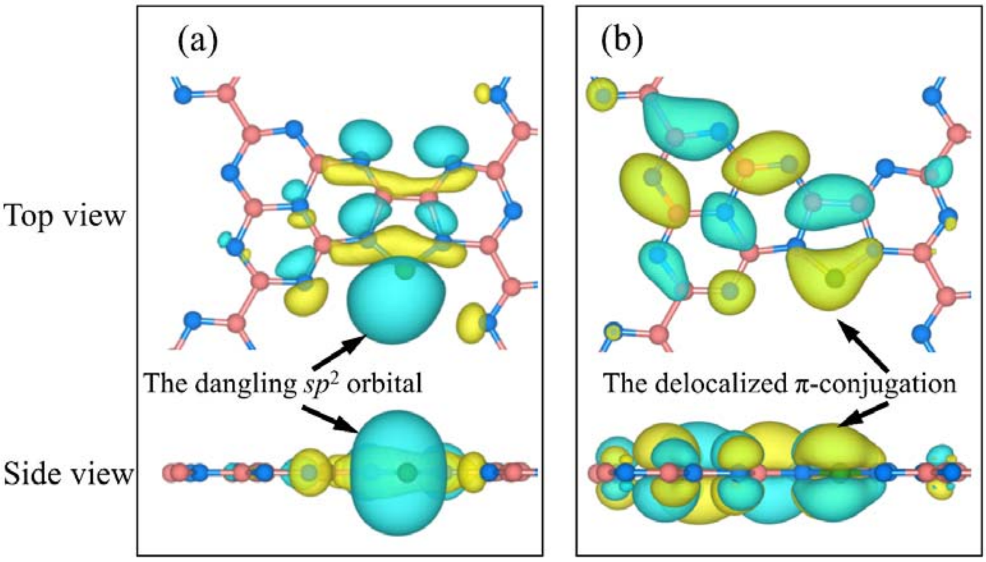

Figure S7. (a) The unoccupied band and (b) occupied band of B@*g*-C_9N_{10}. The cyan and yellow region represent the phases of orbitals. The isosurface value is set to 5×10^{-5} a.u. The pink, blue, and green balls denote carbon, nitrogen, and boron atoms, respectively.

As shown in Figure S7a and S7b, the unoccupied and occupied bands, which obtained from the wave function (the WAVECAR file) at the Γ point in the real space via VASPKIT,[6] are mapped on the skeleton of B@g-C_9N_{10}. The orbital of the doped boron atom (see Figure S7a with arrows pointed), exhibits the typical dangling sp^2 shape, whereas the yellow and cyan ribbons are the typical σ bonding orbitals between the boron and nitrogen atoms, as well as the carbon and nitrogen atoms. Figure S7b presents another type of orbital where the same phases (cyan and cyan, or yellow and yellow) overlap, while these orbitals are separated by the nodes along the bond axis, which are the typical delocalized π-conjugated orbitals between the boron and nitrogen atoms, as well as the carbon and nitrogen atoms.

Table S3. The binding energy of transition metal on *g*-C_2N (cited from Ref. 7)

TM-C_2N	Cr	Mn	Fe	Co	Ni
E_b (eV)	−4.91	−5.41	−6.10	−6.34	−6.67

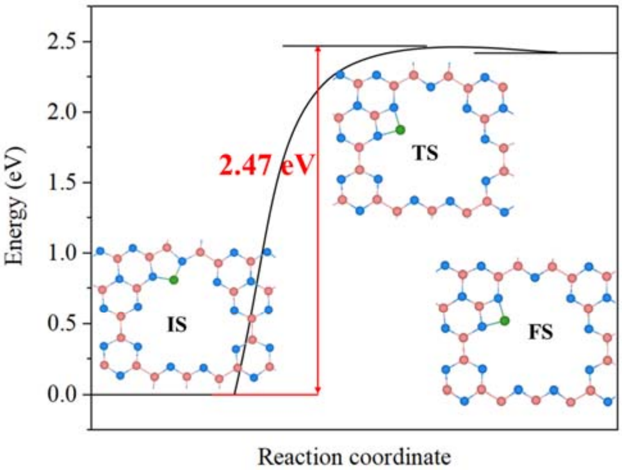

Figure S8. The minimum energy path for the diffusion of B from site 1 to site 2. The inset shows the structures of initial state (IS), transition state (TS), and final state (FS) of B@C_9N_{10}. The pink, blue, and green balls denote carbon, nitrogen, and boron atoms, respectively.

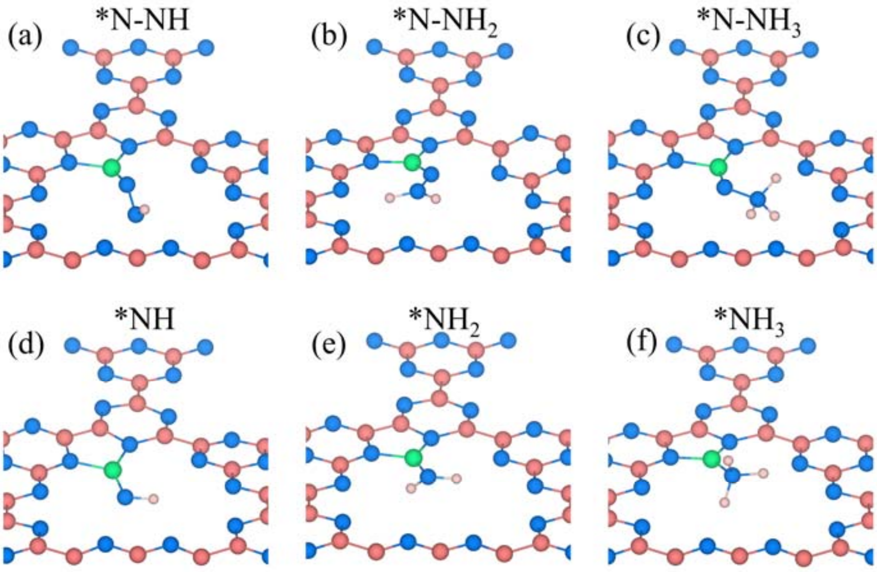

Figure S9. The intermediates of NRR along distal pathway. The pink, blue, and green balls denote carbon, nitrogen, and boron atoms, respectively.

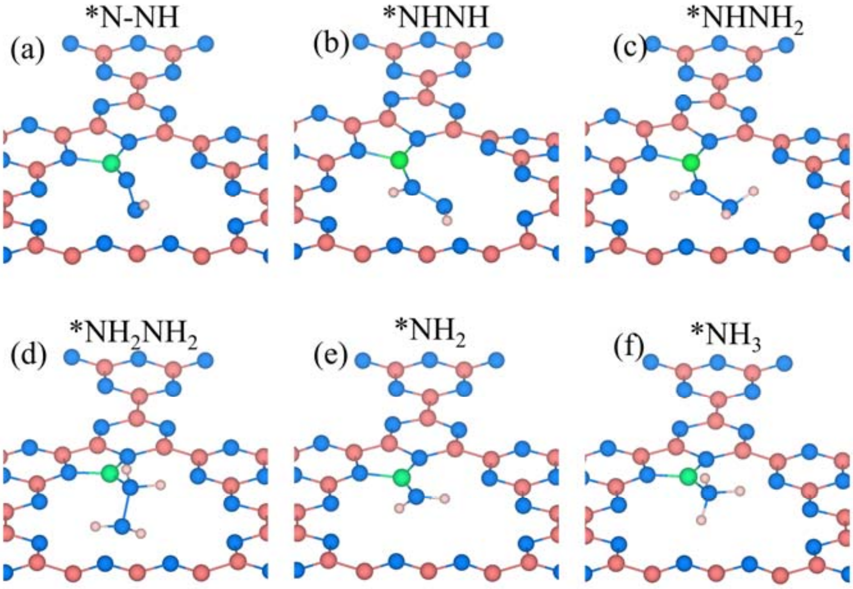

Figure S10. The intermediates of NRR along alternative pathway. The pink, blue, and green balls denote carbon, nitrogen, and boron atoms, respectively.

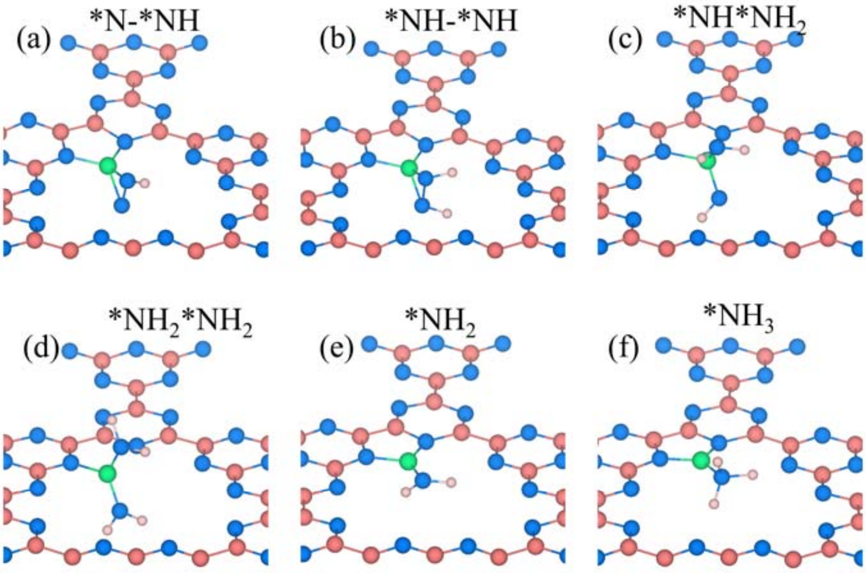

Figure S11. The intermediates of NRR along enzymatic pathway. The pink, blue, and green balls denote carbon, nitrogen, and boron atoms, respectively.

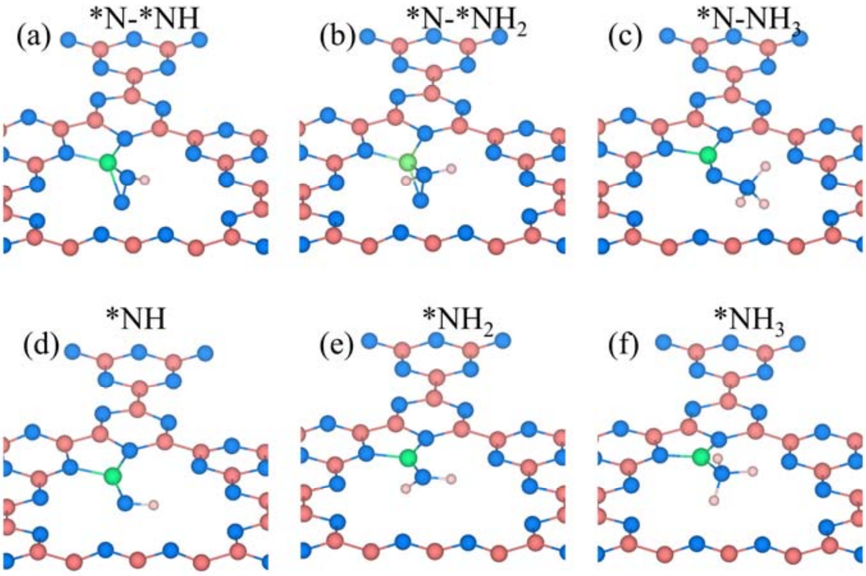

Figure S12. The intermediates of NRR along consecutive pathway. The pink, blue, and green balls denote carbon, nitrogen, and boron atoms, respectively.

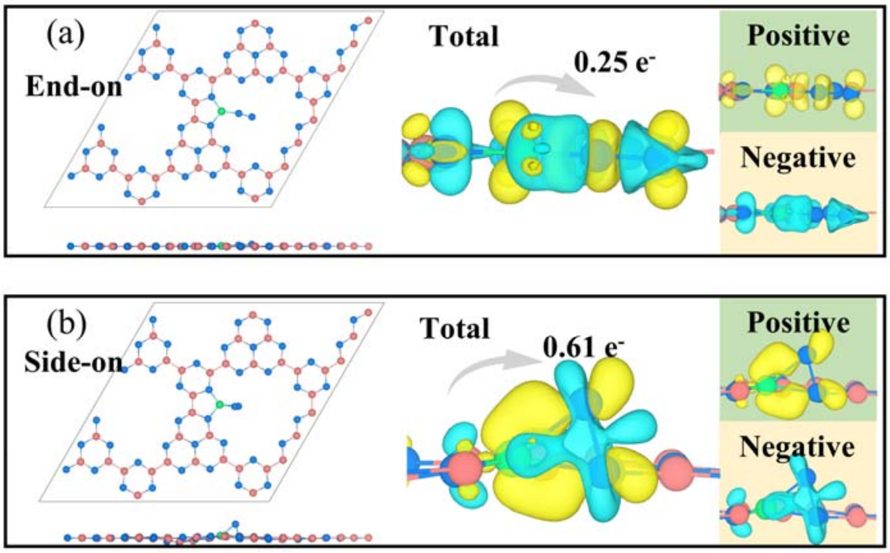

Figure S13. Optimized structures of N_2 adsorption on B@*g*-C_9N_{10} through (a) end-on and (b) side-on configuration, and corresponding difference charge density. Isosurface value is set to 0.05 e/Å^3 and the positive and negative charges are indicated by yellow and cyan, respectively. The pink, blue, and green balls denote carbon, nitrogen, and boron atoms, respectively.

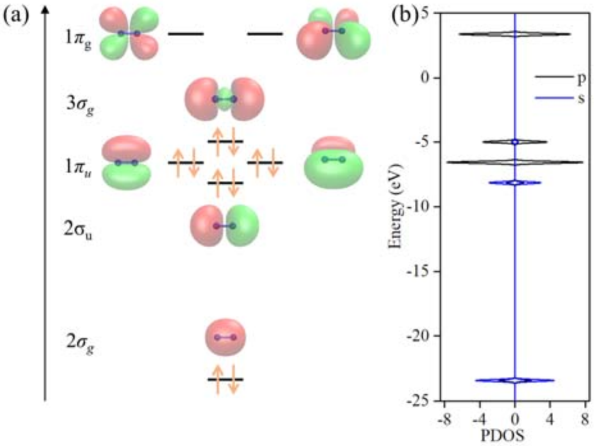

Figure S14. (a) Molecular orbital and (b) The projected density of states (PDOS) of free N_2. The red and green regions represent the phase of orbitals.

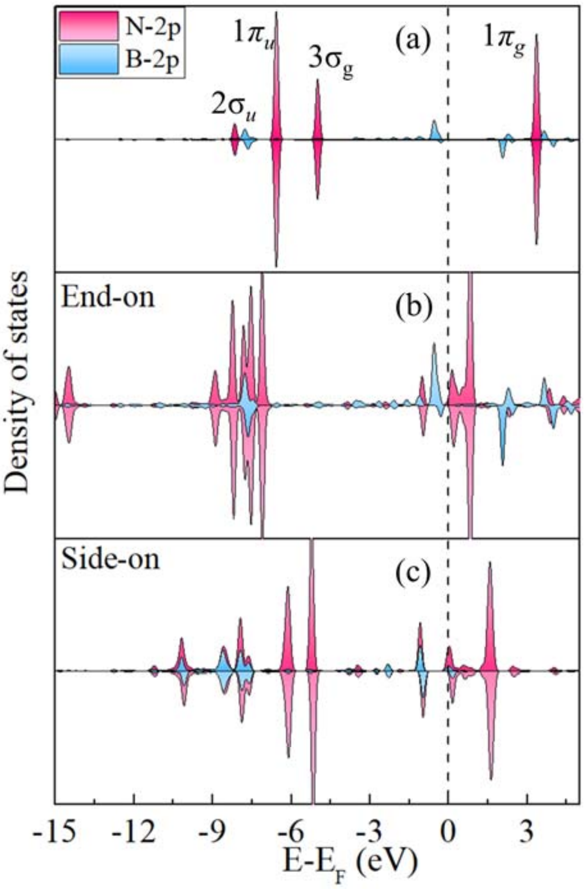

Figure S15. The projected density of states (PDOS) of (a) B@*g*-C_9N_{10} and free N_2. Whereas N_2 adsorbed B@*g*-C_9N_{10} with (b) end-on and (c) side-on configuration.

Table S4. The charge distribution of B in all intermediates along four pathways. The numbers denote the elementary steps along four pathways.

	0	1	2	3	4	5	6
Distal	−1.70	−1.68	−1.59	−1.49	−1.36	−1.76	−1.79
Alternating	−1.70	−1.68	−1.54	−1.44	−1.61	−1.76	−1.79
Enzymatic	−1.57	−1.67	−1.61	−1.65	−1.82	−1.76	−1.79
Consecutive	−1.57	−1.67	−1.72	−1.49	−1.36	−1.76	−1.79

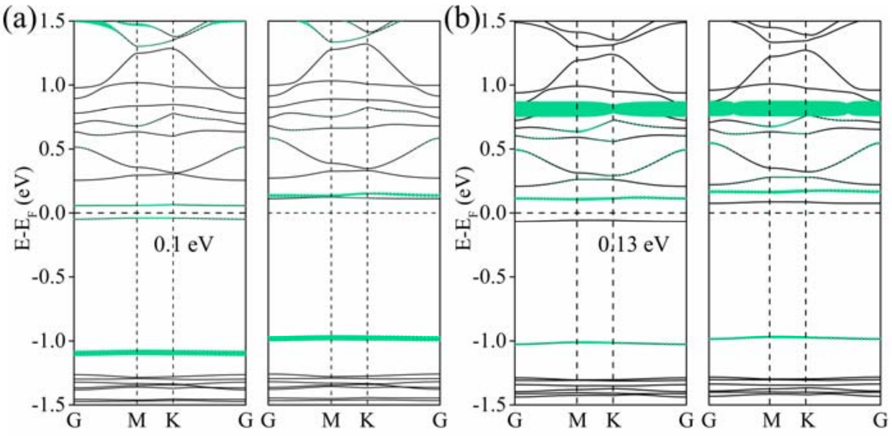

Figure S16. The projected band structure of (a) end-on and (b) side-on N_2 on B@*g*-C_9N_{10}. The green color denotes the N_2 states. The Fermi level is set to zero.

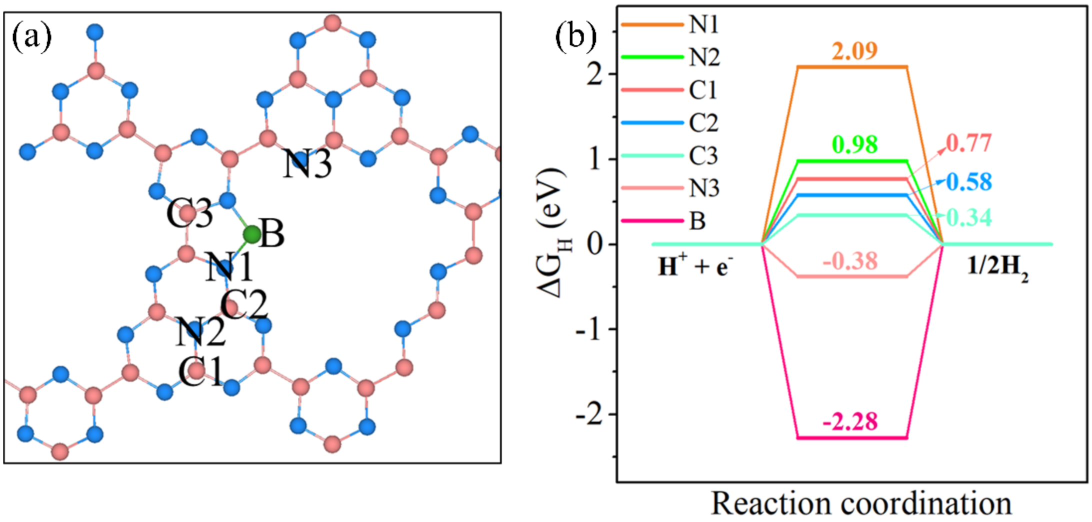

Figure S17. (a) The respective seven possible H adsorption site on B@*g*-C_9N_{10}. The pink, blue, and green balls denote carbon, nitrogen, and boron atoms, respectively. (b) The Gibbs free energy profile of hydrogen evolution reaction (HER) on seven possible site of B@*g*-C_9N_{10}.

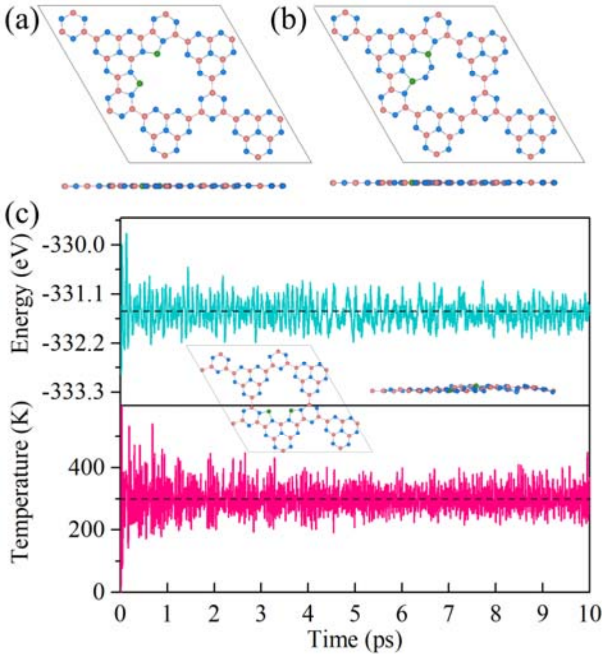

Figure S18. The structure of (a) pristine and (b) N_2 adsorbed DB@*g*-C_9N_{10}. (c) Energy and temperature variation of DB@*g*-C_9N_{10} against AIMD time for 10 ps under 300 K. The inset is the configuration of DB@*g*-C_9N_{10} after AIMD simulation.

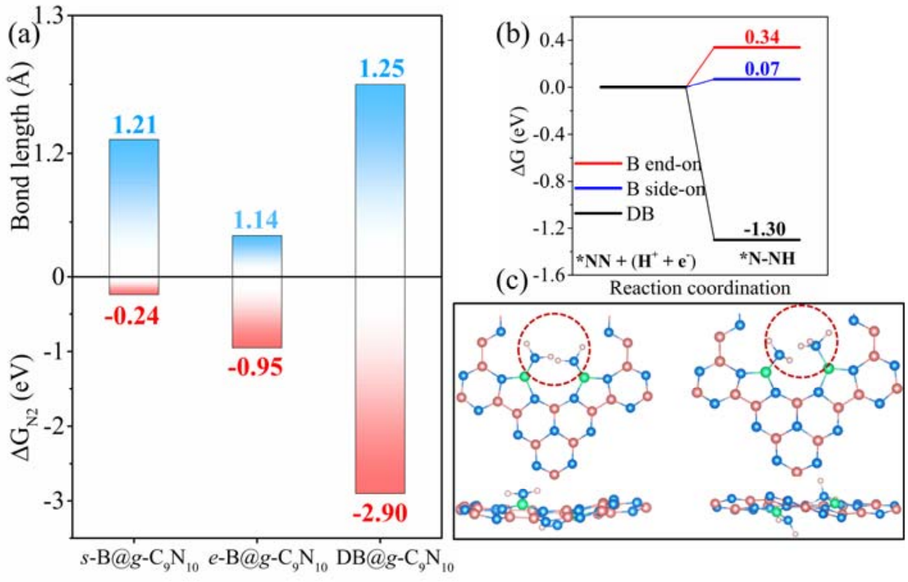

Figure S19. (a) The elongated N≡N bond length and Gibbs free energy of N_2 on B@*g*-C_9N_{10} and DB@*g*-C_9N_{10}. (b) Gibbs energy profile of the first hydrogenation of N_2 on B@*g*-C_9N_{10} and DB@*g*-C_9N_{10}. (c) Structure configuration of *N*N and *N*NH on DB@*g*-C_9N_{10}. The pink, blue, and green balls denote carbon, nitrogen, and boron atoms, respectively.

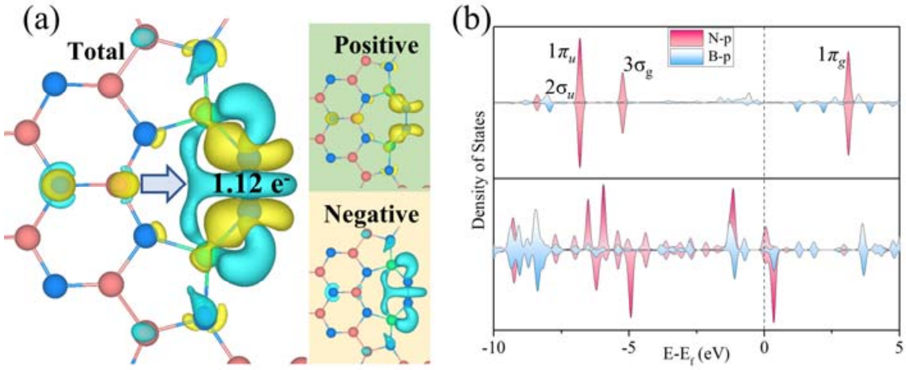

Figure S20. The charge density difference of N_2 on DB@*g*-C_9N_{10}. Isosurface value is set to 0.05 e/Å^3 and the positive and negative charges are indicated by yellow and cyan, respectively. The pink, blue, and green balls denote carbon, nitrogen, and boron atoms, respectively. (b) The projected density of states of B@*g*-C_9N_{10}, free N_2 and N_2 adsorbed DB@*g*-C_9N_{10}.

References

1. J. Li, C. Cao, J. Hao, H. Qiu, Y. Xu and H. Zhu, *Diamond Relat. Mater.*, 2006, **15**, 1593-1600.
2. X. Zhao, Y. Zhao, H. Tan, H. Sun, X. Qin, W. Ho, M. Zhou, J. Lin and Y. Li, *Sci. Bull.*, 2021, **66**, 1764-1772.
3. P. Puthiaraj, S.-S. Kim and W.-S. Ahn, *Chem. Eng. J.*, 2016, **283**, 184-192.
4. K. Kailasam, J. Schmidt, H. Bildirir, G. Zhang, S. Blechert, X. Wang and A. Thomas, *Macromolecular Rapid Communications*, 2013, **34**, 1008-1013.
5. K. Kailasam, M. B. Mesch, L. Möhlmann, M. Baar, S. Blechert, M. Schwarze, M. Schröder, R. Schomäcker, J. Senker and A. Thomas, *Energy Technology*, 2016, **4**, 744-750.
6. V. Wang, N. Xu, J.-C. Liu, G. Tang and W.-T. Geng, *Comput. Phys. Commun.*, 2021, **267**, 108033.
7. Z. W. Chen, J.-M. Yan and Q. Jiang, *Small Methods*, 2019, **3**, 1800291.